Available online at www.sciencedirect.com
ScienceDirect
Deep-Sea Research II 54 (2007) 1029–1044
DEEP-SEA RESEARCH PART II
www.elsevier.com/locate/dsr2

A one-dimensional simulation of biological production in two contrasting mesoscale eddies in the south eastern Indian Ocean

J.E. Greenwood[a,*], M. Feng[a], A.M. Waite[b]

[a]*CSIRO Marine and Atmospheric Research, Floreat, WA, Australia*
[b]*School of Environmental Systems Engineering, University of Western Australia, 35 Stirling Hwy, Crawley 6009, WA, Australia*

Received 21 February 2006; received in revised form 1 July 2006; accepted 20 October 2006
Available online 21 June 2007

Abstract

The question of why anticyclonic eddies appearing along the coast of Western Australia tend to be more productive, and have higher phytoplankton biomass than the cyclonic eddies, remains open. Here we present results from a one-dimensional physical–biological model that explores several possible explanations. In particular, we examine the influence of nutrient conditions during eddy formation and subsequent vertical mixing on the biological production of two counter-rotating mesoscale eddies sampled off Western Australia during October 2003. Observed differences in primary production between the two eddies cannot be adequately explained in the model by differences in mixed-layer depth and vertical nutrient flux. Instead, entrainment of productive shelf waters during the formation of the anticyclonic eddy is suggested to account for up to three quarters of the primary production within the eddy as it moves off-shore. At the same time, the longer residence time of sinking detritus within the deep mixed layer of the anticyclonic eddy is shown to increase the importance of regenerated nitrogen and contribute to its enhanced production. A general under-estimation of production is discussed in the context of biological and physical processes not resolved by the model.

Keywords: Indian Ocean; Leeuwin Current; Eddy; Biogeochemistry; Modelling

1. Introduction

The impact of mesoscale eddies on primary production is generally thought to hinge on the increased nutrient supply from productive cyclonic eddies, while anticyclonic eddies are relatively unproductive nutrient deserts (McGillicuddy et al., 1999). In contrast, in the Leeuwin Current (LC) off Western Australia, anticyclonic warm-core (WC) eddies tend to have higher phytoplankton biomass (Moore et al., 2007; Feng et al., 2007) and be more productive (Waite et al., 2007), than the cyclonic cold-core (CC) eddies. An adequate explanation to account for this difference is yet to be settled. The fact that the anticyclonic eddies move productive waters from the continental shelf offshore may be one of the factors driving the increased productivity of LC-WC eddies. The role of vertical mixing within the surface mixed layer of the WC and CC eddies in supporting continuing production is not clear, but is thought to support an important population of large diatoms which may drive enhanced production (Thompson et al., 2007; Waite et al., 2007).

*Corresponding author. Tel.: +61 89333 6564; fax: +61 89333 6555.
E-mail address: Jim.Greenwood@csiro.au (J.E. Greenwood).

0967-0645/$ - see front matter © 2007 Elsevier Ltd. All rights reserved.
doi:10.1016/j.dsr2.2006.10.004

The LC has the strongest eddy kinetic energy among all mid-latitude eastern-boundary current systems (Feng et al., 2005). In the LC eddy systems the CC eddies are often sub-surface features that spin up from the Leeuwin undercurrent, with little active upwelling (Rennie et al., 2007), while the WC eddies draw waters from the LC proper (Feng et al., 2007), and have statistically higher primary production as estimated from remote sensing (Moore et al., 2007). Understanding what makes the WC eddies so productive is thus of significant importance in terms of predicting the productivity of the LC overall. Some investigators have speculated that diapycnal mixing is a key source of nitrogen to the LC-WC eddies (Moore et al., 2007). Other possible inputs include incorporation of nitrate into the original eddy as it was formed, regional subduction of nitrogen-rich waters below and into the eddy, nitrogen fixation, and entrainment via the inter-eddy jet. The first intensive field sampling of two counter-rotating LC eddies during October 2003 (Waite et al., 2007) provided a unique opportunity to estimate nutrient fluxes from field data, and assess the potential importance of several key nutrient sources in driving the productivity observed. Satellite data show that this eddy pair evolved from meanders in the LC during May and fully detached from the current around the end of August (Feng et al., 2007). The two eddies are distinctly different with the water in the mixed layer of the anticyclonic eddy thought to originate from the LC, while the water at the core of the cyclonic eddy is similar to surrounding open-ocean water (Feng et al., 2007). The WC eddy was characterized in October 2003 by high surface chlorophyll and high primary production. Nitrate was probably the nutrient-limiting phytoplankton biomass at this time and was mostly non-detectable to approximately 275 m at the centre of the WC eddy, and 100 m at the centre of the CC eddy (Thompson et al., 2007).

A variety of one-dimensional (1-D) physical–biogeochemical models have been used in recent years to simulate the dynamics of upper-ocean plankton ecosystems (e.g., Doney et al., 1996; Oguz et al., 1996; Fennel et al., 2002). While their success in reproducing observations relies in part on the assumption that horizontal processes are relatively unimportant, by simplifying the physics they have also proved useful as a first step in understanding nutrient supply mechanisms associated with more complex mesoscale dynamical processes (e.g., McGillicuddy et al., 1995; Martin and Pondaven, 2003). Here, we present results from a number of idealized simulations designed specifically to examine the relative importance of diapycnal mixing and initial nutrient conditions on the primary production of the two counter-rotating LC eddies (Fig. 1) sampled during October 2003 (Waite et al., 2007). We base our main analysis on vertical flux estimates within the core, or centre, of each eddy and compare model output with physical and biological measurements made at the centre of the WC eddy between 1 and 10 October 2003, and at the centre of the CC eddy between 11 and 21 October 2003. We also discuss the role of regenerated nitrogen. This paper is primarily intended as a process study to investigate the relative importance of these key nutrient supply mechanisms, and not as an attempt to accurately simulate the observations.

2. Assumptions of the 1-D approach

Our 1-D Lagrangian approach focuses on the primary mechanisms limiting vertical nutrient flux into the eddy and initial nutrient incorporation into the forming eddy. Lateral processes in the eddy field such as vertical circulation and horizontal mixing are neglected. This is justified by the fact that within the eddy perimeters, the mixed-layer properties are homogeneous and show little temporal variation during the course of the eddy cruise (Feng et al., 2007).

A finite-size Lyapunov exponent (FSLE) of the 2-D sea-surface geostrophic velocity field derived from satellite altimetry is used to quantify the stable and unstable manifolds of the surface flow during the eddy cruise (Feng, 2006). Low FSLE is observed in the centre of both eddies (Fig. 2), indicating a low stirring rate consistent with the water mass analysis. In addition, both eddies are bounded by well-defined stable/unstable manifolds, indicating there is little exchange across the eddy perimeters (Fig. 2). The southward inter-eddy jet or surface warm jet (SWJ) (Fig. 1) is denoted by an unstable manifold exit from a hyperbolic point (interception of stable and unstable manifolds) north of the two eddies. The fate of the SWJ is uncertain based on the FSLE analysis. The intrusion of the Subtropical Front (STF) waters southeast of the WC eddy is denoted by strong tangling of the manifolds. Although this analysis represents only a ‘snap shot’ of the eddy dynamics, and is restricted by the resolution of the altimeter data (approx. 30 km), which may not fully

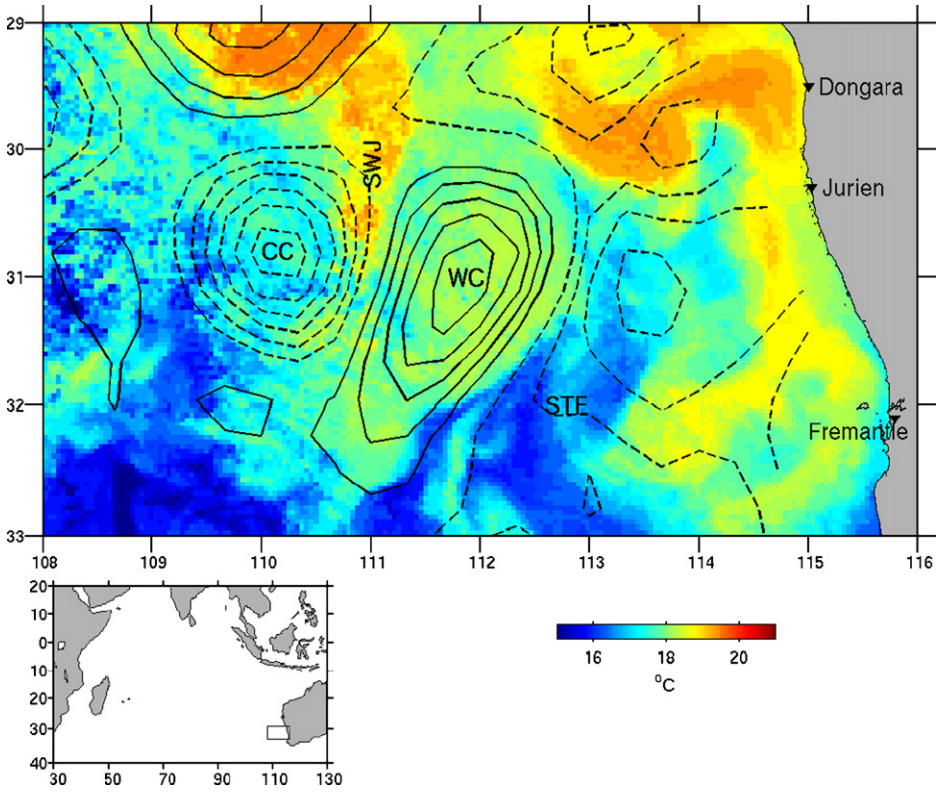

Fig. 1. Sea-surface height anomaly (contour) and a 3-day SST composite (colour) around 10 October 2003 off southwest Western Australian coast. Solid (dashed) contours are positive (negative) sea-level anomalies at 5-cm intervals from 5 (−5) cm, and the zero contour is not plotted. The inset denotes the location of the survey domain in the Indian Ocean. WC and CC denote the warm-core and cold-core eddies, and STF and SWJ denote the subtropical front waters and the surface warm jet, respectively.

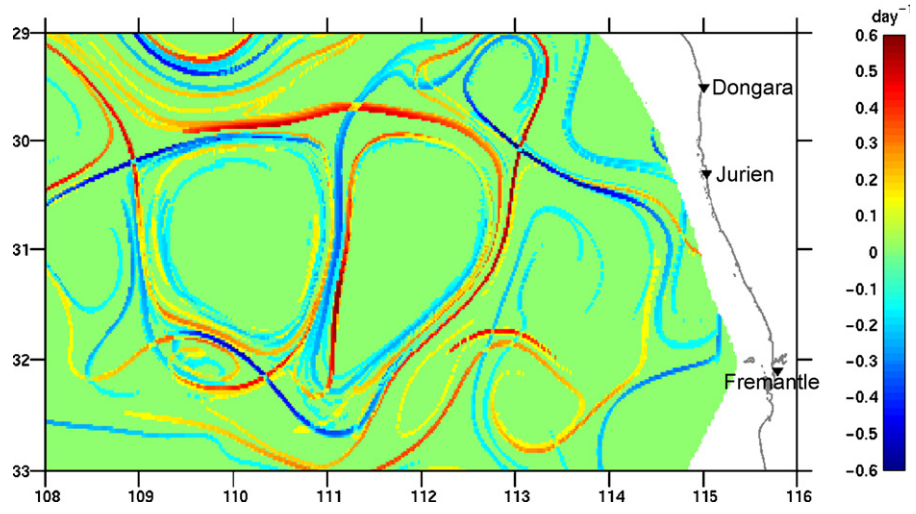

Fig. 2. Spatial distribution of the forward (positive) and backward (negative) FSLE of the surface geostrophic current field around 10 October 2003. High positive values denote the stable manifolds of the flow field, and high negative values the unstable manifolds.

resolve the eddy dynamics (approx. 70 km in diameter), it provides some justification for our simplified approach.

Further reassurance that the eddies can be reasonably viewed in a Lagrangian frame throughout our experiment is provided by the temporal

evolution of the temperature field at 200 m (Fig. 3) obtained from an analysis system that uses historical data (including some limited sampling of both types of eddy) to statistically infer sub-surface ocean properties from surface observations of sea-surface height anomaly and temperature (K.R. Ridgway and J. R. Dunn, CSIRO Project Report, 2002). The two eddies start to form from the LC in May 2003 and fully detach from the current in late August/early September (Feng et al., 2007). Following detachment, the structure of the two eddies is maintained (Fig. 3), suggesting that there is little exchange between the centre of the eddy and the surrounding water. A similar result is found from the analysis of float data for eddies in the Sargasso Sea showing that waters within them can be trapped for long periods (Richardson, 1993).

3. Model description

A 1-D physical–biogeochemical model is used to represent the upper 500 m at the centre of each eddy, with a vertical resolution of 10 m throughout the water column except in the upper 10 m, where vertical resolution was increased to 2.5 m. Atmospheric forcing is arranged to represent the varying conditions experienced by the two eddies as they propagate off-shore, and is the same for all simulations. The lower boundary of the model domain is left open to allow diffusive fluxes and sinking particles to cross the base of the model. The values of biological scalars are fixed at the lower boundary implying a dissolved-nutrient flux into the model domain determined by the concentration gradient and the background diffusion coefficient.

3.1. Physical model

In the physical model, vertical mixing is calculated using the k–ε mixing scheme (Burchard and Baumert, 1995) forced with 6 hourly fluxes of long- and short-wave radiation, wind stress, evaporation and precipitation from the National Centre of Environmental Prediction (NCEP; Kalnay et al., 1996) spatially interpolated along the track of the WC eddy. Heat penetration of insolation is described by a double exponential (Kraus, 1972) that includes a short- and long-wave component of solar radiation. The effect of surface forcing becomes negligible below the thermocline and turbulent kinetic energy tends toward zero. In deeper layers a minimum value for eddy diffusivity of

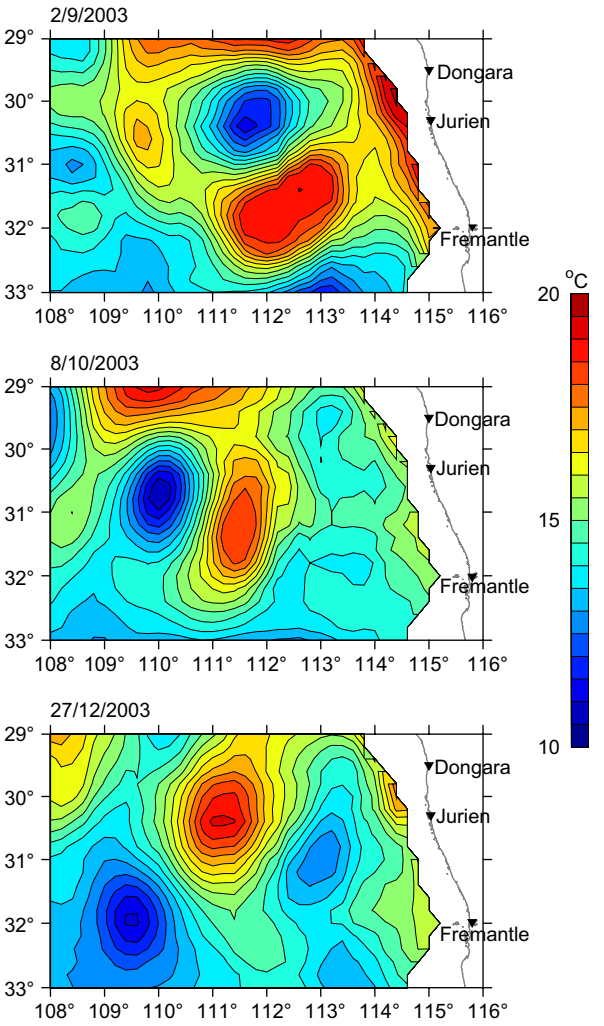

Fig. 3. Temporal evolution of a statistically inferred temperature field at 200 m depth from September to December 2003. The high- and low-temperature cores in the three panels denote the warm-core (WC) and cold-core (CC) eddies sampled during the October 2003 cruise. Also note that while the eddy pair moves slowly westward, the CC eddy also revolves around the WC eddy anti-cyclonically (Feng et al., 2007).

$1 \times 10^{-5}\,m^2\,s^{-1}$ was set for both the WC and CC eddy. Model temperature and salinity were initialized for 28 May 2003 with statistically inferred profiles (Fig. 6A) derived using the same analysis system described in Section 2, and used to produce Fig. 3. Each simulation is constrained by weak temperature and salinity restoration, with a restoration time constant of 100 d, to vertical profiles measured at the eddy centres during the October 2003 cruise. The need for this relatively gentle correction is thought to originate from either

unresolved air-sea heat fluxes, or horizontal processes that are missing in our 1-D approach. Although we found the model to perform reasonably well without this added constraint, mixed-layer depths tended to be overestimated by the model especially for the CC eddy (not shown).

Near the end of September 2003, the wind field off WA experiences a transition from dominantly eastward to dominantly northward (Fig. 4). The net surface heat flux also has a transition near the end of September 2003 from persistent heat loss during the austral winter to no loss or alternating fluxes throughout the spring, until late December when summer heating sets in (Fig. 4). There is always a net freshwater loss at the air–sea interface, with stronger losses during November–December (Fig. 4). During the eddy cruise in October, surface wind and buoyancy fluxes are both weak.

3.2. Biological model

The nitrogen based biological model includes only four state variables: dissolved inorganic nitrogen (DIN), phytoplankton (P), zooplankton (Zoo), and sinking detritus (D). Phytoplankton growth and zooplankton grazing are based on simple empirical descriptions (Table 1). Photosynthetically active radiation (PAR) is assumed to be 43% of the net short-wave radiation provided by NCEP. Most parameter values for the biological model were set a priori according to commonly used literature values (Table 2). Detrital sinking speed and decay rate were adjusted manually to obtain realistic values of production and detrital export during October.

We use the model to compare temporal variability at the centre of each eddy between June and December 2003. In total three model runs were performed, one for the CC eddy and two for the WC eddy. Model DIN was initialized using a relationship between temperature and nitrate constructed from observations made in the vicinity of the formation of the two eddies during late autumn/early winter 2003 (Fig. 5). This is a region strongly influenced by the LC and the temperature nutrient relationship is therefore expected to be more appropriate for LC water than for off-shore water. Phytoplankton, zooplankton and detrital biomass were initialized with small constant values. To establish initial values for the biological variables the model was run repeatedly for each eddy with constant forcing using the appropriate mean vertical profiles of eddy diffusivity and temperature calculated by the physical model, and mean daily radiation for May 2003, until a pseudo steady state was observed (obtained after 90 days). In the first pair of runs (WC1 and CC1) surface DIN was allowed to evolve freely during this 'spin-up' period, and tended toward zero, while deeper concentrations (below 100 m for the CC eddy, and below 200 m for the WC eddy) were constrained by gentle relaxation toward the initial profile (Figs. 6 and 7). An additional run of the WC eddy simulation (WC2) employed 100 day relaxation of DIN towards the initial profile throughout the entire water column during this 90-day 'spin up' period. In this case, relaxation was arranged to ensure that surface DIN concentrations consistent with the observed nitrogen temperature relationship were maintained. The purpose of this second WC eddy simulation was to imitate continued flushing of the WC eddy with relatively high nutrient surface waters during its formation (Fig. 7A). It should be noted that this has the effect of elevating not only initial DIN concentrations in WC2 but also initial concentrations of phytoplankton, zooplankton and detritus. The end position of these 'spin-up' runs provided the initial values of the biological scalars for the main runs where they were allowed to evolve freely unless otherwise stated.

4. Results

4.1. Physics

Comparison of vertical profiles of temperature and salinity measured at the centre of each eddy during October with mean profiles simulated by the model during the same period, shows that the vertical structure of both eddies is well represented by the model (Figs. 8B and 9B). This is consistent with the good agreement in mixed-layer depth calculated from model and observed data during October (Fig. 11). The general temporal trend in surface temperature simulated by the model for the WC eddy also agrees well with satellite observations (Fig. 10). The high-frequency variability seen in the satellite data is not reproduced by the model, although we suspect that some of this variability results from errors in the satellite data itself. The model performs less well in reproducing the temporal evolution of the surface temperature for the CC eddy, apparently cooling too rapidly between June and September (Fig. 10). Despite

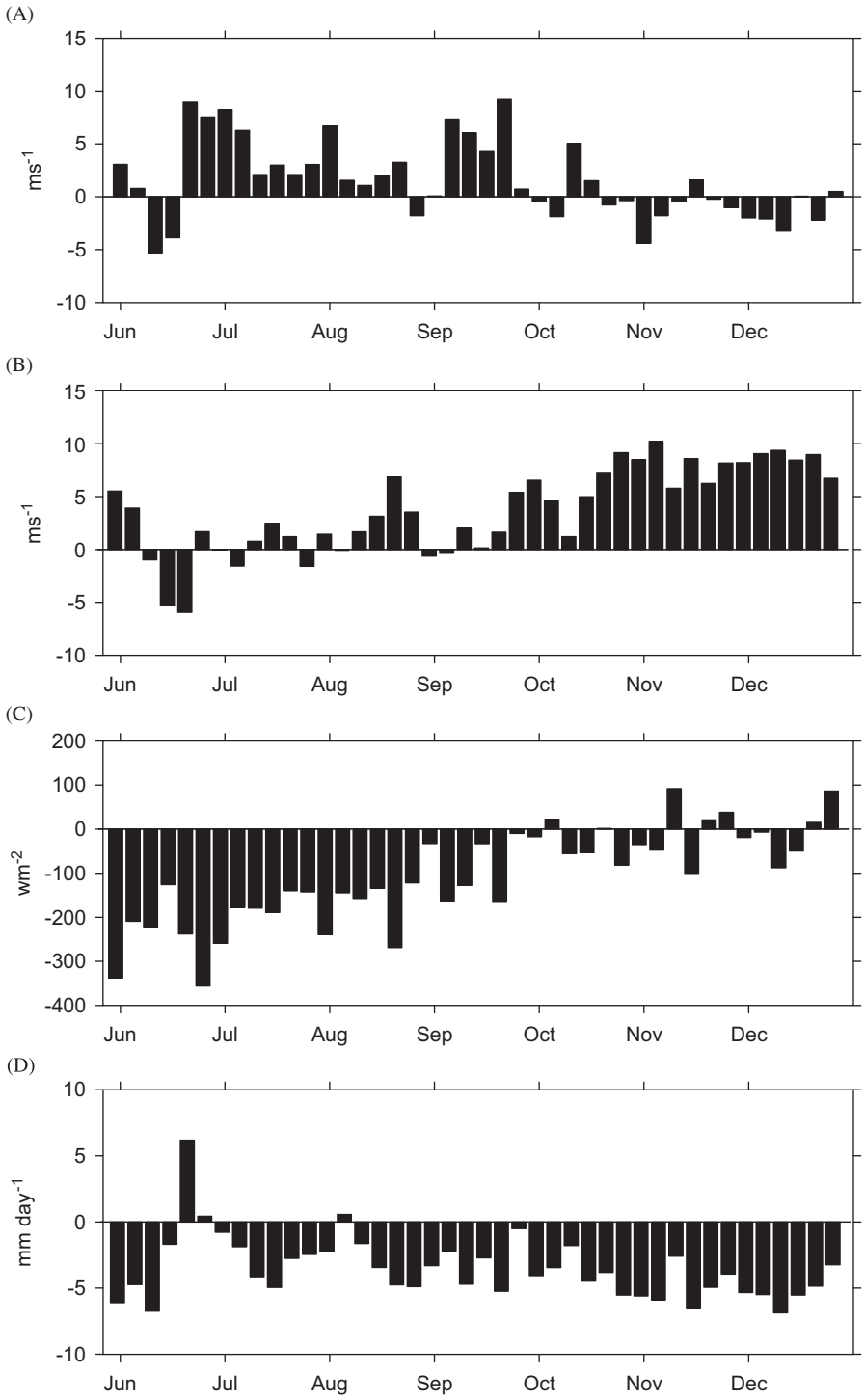

Fig. 4. Five-day averages of (A) zonal wind speed, (B) meridional wind speed, (C) net surface heat flux, and (D) net freshwater flux from the NCEP reanalysis product between June and December 2003.

a continuing underestimation of temperature by the model of around 1.5°, caused by the early rapid cooling, the warming trend in temperature between October and December is reasonably well represented by the model (Fig. 10). The under estimation of surface temperature during October is consistent

Table 1
The rate equations used in the biological model[a]

State variable	Rate equations
Phytoplankton N (mmol N m^{-3})	$\frac{\delta P}{\delta t} = \frac{\delta}{\delta z}\left(K_z \frac{\delta P}{\delta z}\right) - \omega_p \frac{\delta P}{\delta z} + R_{max} P_{min}\left[\frac{DIN}{DIN + ks_p}, 1 - \exp(-\alpha.PAR/R_{max})\right] - m_p P - G$
	$R_{max} = P_{max} \frac{ChlN}{(CN\,mw\,C)} \exp(ktT)$
Zooplankton N (mmol N m^{-3})	$\frac{dZoo}{dt} = \frac{\delta}{\delta z}\left(K_z \frac{\delta Zoo}{\delta t}\right) + \gamma G - m_{zoo} Zoo^2 - rZoo$
	$G = G_{max} Zoo\left(\frac{P}{P + ks_{zoo}}\right), \quad rZoo = k_{resp}\,Zoo + k_{food}\,grazing$
Detritus (mmol N m^{-3})	$\frac{\delta D}{\delta t} = \frac{\delta}{\delta z}\left(K_z \frac{\delta D}{\delta z}\right) - \omega_D \frac{\delta D}{\delta z} + (1-\gamma)G + m_{zoo} Zoo^2 + m_p P - R_D D$
DIN (mmol N m^{-3})	$\frac{\delta DIN}{\delta t} = \frac{\delta}{\delta z}\left(K_z \frac{\delta DIN}{\delta z}\right) - R_{max} P_{min}\left[\frac{DIN}{DIN + ks_p}, 1 - \exp(-\alpha\,PAR/R_{max})\right] + R_D D + rZoo$

[a] K_z is vertical eddy diffusivity, T is temperature, and z is water depth. All other variables and parameters are defined either in the text or in Table 2.

Table 2
Parameters used in the biological model

Parameter	Description	Value	Units
ω_p	Phytoplankton sinking speed	1.0(c)	m day^{-1}
ks_p	Half saturation of DIN uptake	0.5(b,c)	mmol m^{-3}
α	Photosynthetic efficiency	0.003(a)	(Wm^{-2})$^{-1}$h^{-1}
m_p	Phytoplankton mortality rate	0.05(a,c)	day^{-1}
P_{max}	Maximum photosynthetic rate	1.0	gC gChl^{-1} h^{-1}
ChlN	Chlorophyll nitrogen ratio	2.0(c)	gChl mol N^{-1}
CN	Carbon nitrogen ratio	6.6(b)	mol C mol N^{-1}
mwC	Molecular weight of carbon	12.0	g
kt	Temperature dependence of phytoplankton growth	0.0633(c)	°C^{-1}
γ	Zooplankton assimilation efficiency	0.75(c)	—
m_{zoo}	Zooplankton mortality rate	0.05(c)	day^{-1}
G_{max}	Zooplankton maximum grazing rate	0.7(c)	day^{-1}
ks_{zoo}	Half saturation grazing	0.75(c)	—
k_{resp}	Zooplankton basal respiration rate	0.05(c)	day^{-1}
k_{food}	Part of ingested food respired	0.25(c)	—
ω_D	Detrital sinking speed	10	m day^{-1}
R_D	Detrital decay rate	0.06	day^{-1}
k_d	PAR attenuation coefficient	0.04(b,c)	m^{-1}

Parameters agree with values in common use: (a) Denman and Pena (1999); (b) Spitz et al. (2001); (c) Kantha (2004). The value of P_{max} is based on measurements made during the 2003 eddy crusie (see Thompson et al., 2007). Sinking and detrital decay rates have been tuned for this study.

with the comparison of modelled and observed vertical temperature profiles that suggest the model underestimates the temperature throughout the entire mixed layer of the CC eddy by around 1.5° (Fig. 8B). The reason for the 'over-cooling' seen in the CC eddy model during the first part of the simulation is unclear, but suggests that there is either a problem with the resolution of the NCEP

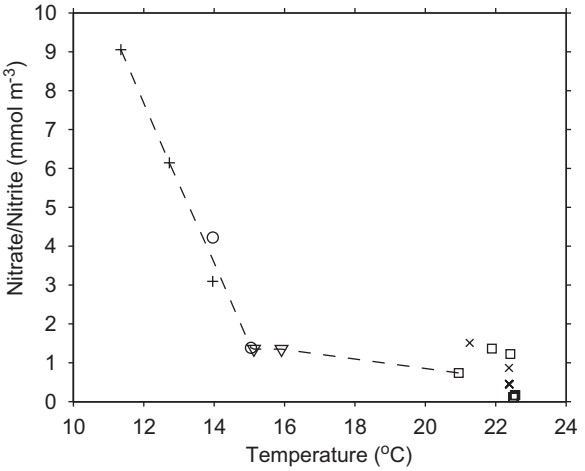

Fig. 5. Temperature–nutrient relationship used to initialize the biological model. The symbols represent samples collected on separate cruises during late autumn and early winter 2003 at three stations, 'D' (31.77S, 115.00E), 'DE' (31.81S, 114.91E), and 'E' (31.86S, 114.79E) in the vicinity of the region where the two eddies formed.

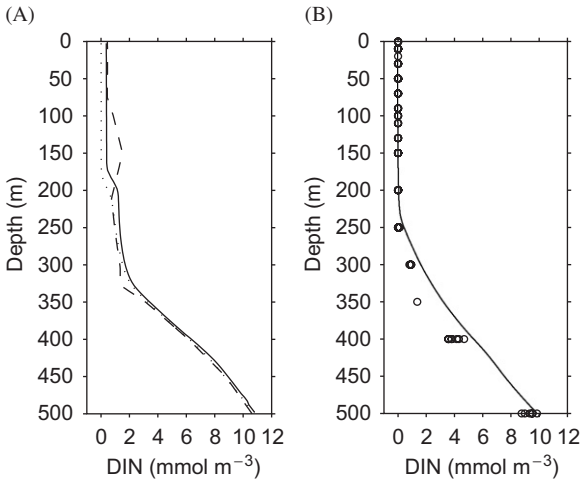

Fig. 7. Vertical DIN profile for the WC eddy in the upper 500 m (A) before (dashed line) and after 90-day spin-up run for WC1 (dotted line) and WC2 (solid line). In (B) the mean model simulated DIN profile during early October (line) is compared with measurements taken during the same period.

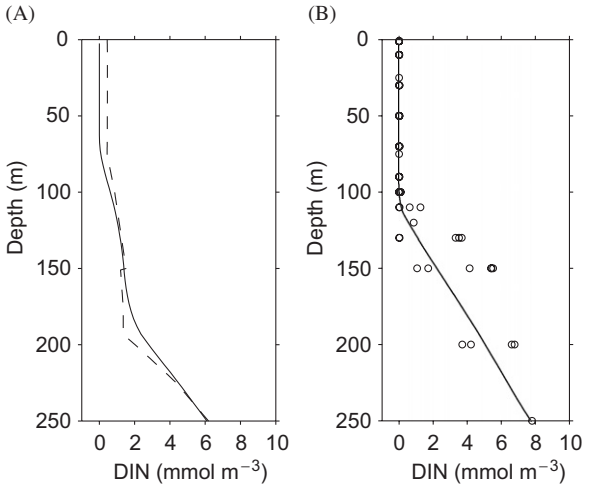

Fig. 6. Vertical DIN profile for the CC eddy in the upper 250 m (A) before (broken line) and after (solid line) 90-day spin-up run. In (B) the mean model simulated DIN profile during early October (line) is compared with measurements taken during the same period.

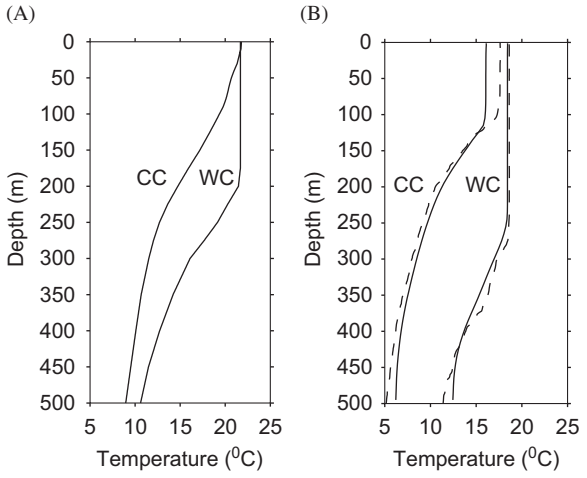

Fig. 8. Vertical temperature profiles at the centre of the WC and CC eddies (A) used to initialize the model, and (B) predicted by the model during early October (solid line) compared with those measured during the same period (dashed line).

surface forcing, or horizontal heat fluxes associated with the CC eddy that are not resolved by our model. It is also worth noting that the model underestimates the mixed-layer salinity of the CC eddy by around 0.1 psu, and fails to reproduce the salinity maximum observed around 300 m depth during October in the WC eddy (Fig. 9).

A deepening in model simulated mixed-layer depth of around 50 m is evident for both eddies between June and September (Fig. 11). This is followed by a gradual shoaling, most noticeable for the CC eddy, which increases toward the end of December. Both the deepening and shoaling of the mixed layer are consistent with trends in surface heat flux (Fig. 4). Fig. 12 shows the temporal and vertical variation in eddy diffusivity predicted by the

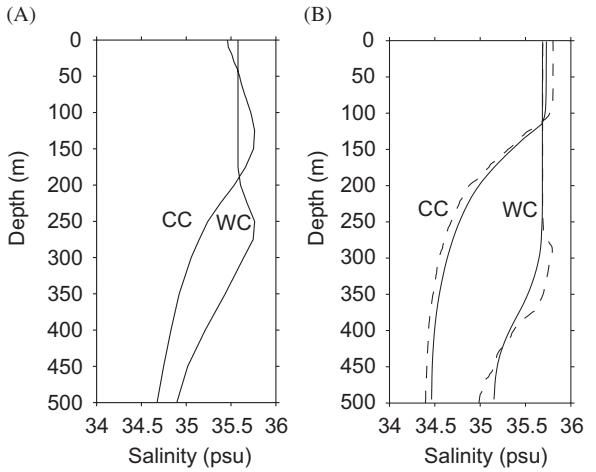

Fig. 9. Vertical salinity profiles at the centre of the WC and CC eddies: (A) used to initialize the model; and (B) predicted by the model during early October (solid line) compared with those measured during the same period (dashed line).

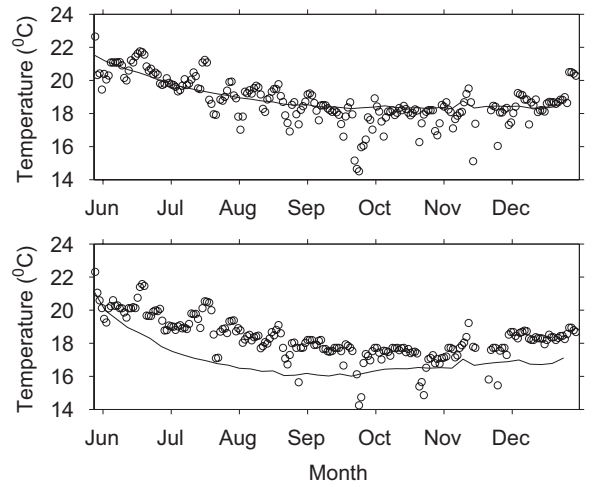

Fig. 10. Variation in model simulated surface temperature at the centre of the WC (upper panel) and CC (lower panel) eddy (lines), compared with satellite-derived SST (symbols), between June and December 2003.

model, highlighting the contrast in vertical mixing between the two eddies. Vertical mixing averaged over the upper 100 m is consistently stronger in the WC eddy, although this difference becomes less pronounced toward the end of the simulation (Fig. 12A). Given the same surface forcing, the extension of enhanced vertical mixing in the WC eddy some 100 m deeper than in the CC eddy during October (Fig. 12B) is consistent with differences in mixed-layer depth between the two simulations (Fig. 11). At 50 m depth, mixing during the first

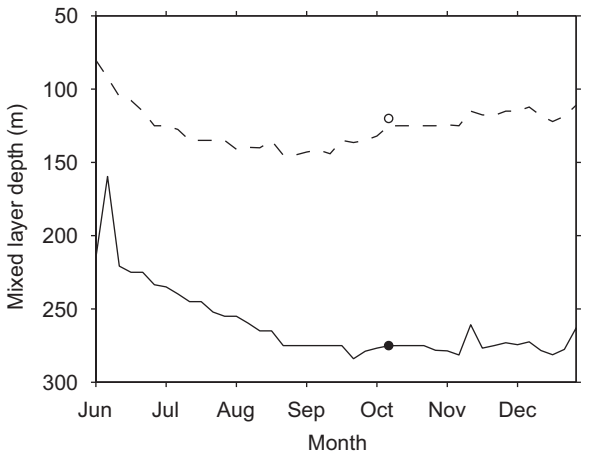

Fig. 11. Variation in model predicted mixed-layer depth (5-day mean) for the WC (solid line), and CC (dashed line), eddies compared with mean observations (standard deviation = 6 m for WC and 11 m for CC) during October 2003 (symbols). Mixed-layer depth is defined by an offset in surface density of $0.125\,kg\,m^{-3}$.

20 days of October is approximately 1.8 times greater in the warm-core eddy than in the CC eddy, at the lower end of the range of mixing ratios derived independently from the vertical variation in phytoplankton physiology and community composition observed at this time (Thompson et al., 2007). Consistent with the variability of the surface forcing, a general weakening in vertical mixing is evident in both eddies from September to November with periods of weaker mixing particularly noticeable during early October and late November (Fig. 12A).

4.2. Nutrients and plankton

Simulated vertical profiles of DIN during the first half of October for the cold-core eddy (CC1) are in good agreement with nitrate observations during the eddy cruise (Fig. 6b). The model was found to perform less well in the case of the WC eddy, under estimating the depth, and over estimating the slope of the nutricline. Therefore, to maintain meaningful fluxes of nitrogen into the mixed layer of the WC eddy, simulated DIN concentrations below 250 m were weakly restored toward observed October values with a relaxation time constant of 1000 days. This relatively minor correction in DIN below the mixed layer was sufficient to achieve a simulated DIN profile, in good agreement with observations (Fig. 7b).

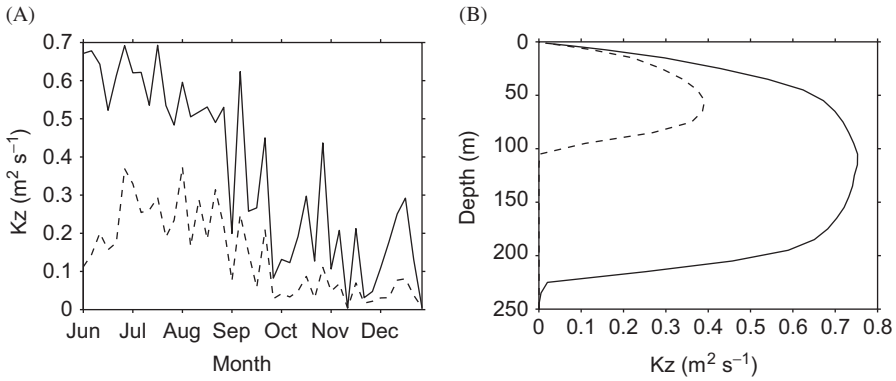

Fig. 12. Temporal and vertical variation in model simulated vertical eddy diffusivity (K_z): (A) averaged over the upper 100 m (5-day mean); and (B) averaged over the first 20 days of October for the WC (solid line) and CC (broken line) eddy.

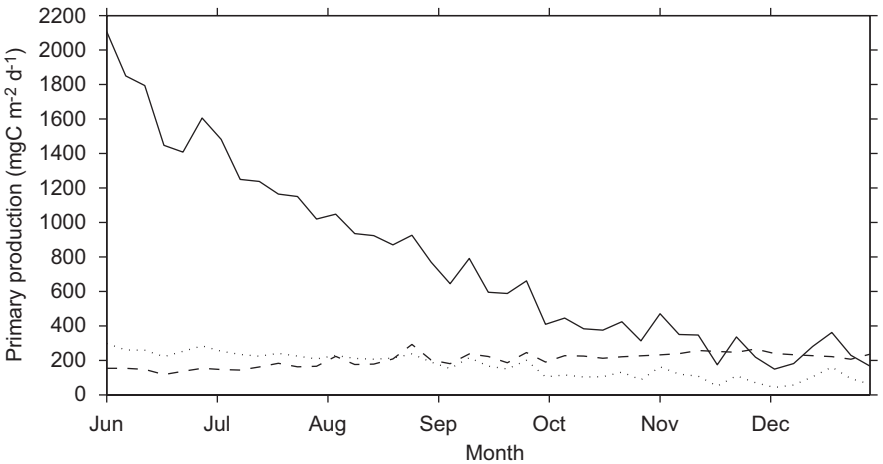

Fig. 13. Variation in depth integrated (0–150 m) primary production (5-day mean) between June and December 2003 simulated by the model for runs WCl (dotted line), WC2 (solid line), and CCl (dashed line).

Initialized with the original temperature–nitrate relationship (WC1 and CC1), depth integrated primary production between June and December in the two eddy simulations show contrasting trends. While the WC eddy simulation shows a steady decrease in production, the CC eddy simulation predicts little change (Fig. 13). The result of these differing trends is that while production in the WC eddy is initially some 50% higher than that in the CC eddy, by mid-August production in the CC eddy begins to exceed that of the WC eddy. During early October, production in the CC eddy closely approaches the observed value (Table 3), but is more than 50% higher than in the WC eddy for which production is vastly underestimated by the model (Table 3). Maintenance of high nutrient surface water during 'spin-up' to create the initial conditions for the second WC eddy simulation (WC2) has a dramatic effect on subsequent production. In this case (WC2), production is around 10 times greater than in the first WC eddy run (WC1) at the beginning of the simulation, decreasing rapidly toward the end of the year. Production in the WC eddy also now exceeds that of the CC eddy until late November when production in the two eddies is comparable (Fig. 13). Simulated production during early October for model runs WC2 and CC1 presents the most realistic result when compared with observations, with production in the WC eddy around 46% higher than in the CC eddy (observations suggest a difference of 44%) (Table 3). Even so, production during October tends to be underestimated by the model for both eddies. Simulated fluxes of detrital nitrogen at 300 m for

Table 3
Comparison of mean depth integrated production, and export flux (at 300 m) simulated by the model and measured (Obs) during early October 2003

	Warm eddy			Cold eddy	
	WC1	WC2	Obs	CC1	Obs
Production (mg C m^{-2} day^{-1})	110 (75–175)	416 (280–645)	449 (267–530)	223 (210–241)	252 (208–281)
Export (mol N m^{-2} day^{-1})	3.0×10^{-4}	7.8×10^{-4}	1.4×10^{-3}	5.0×10^{-4}	1.0×10^{-3}

Numbers in brackets indicate range.

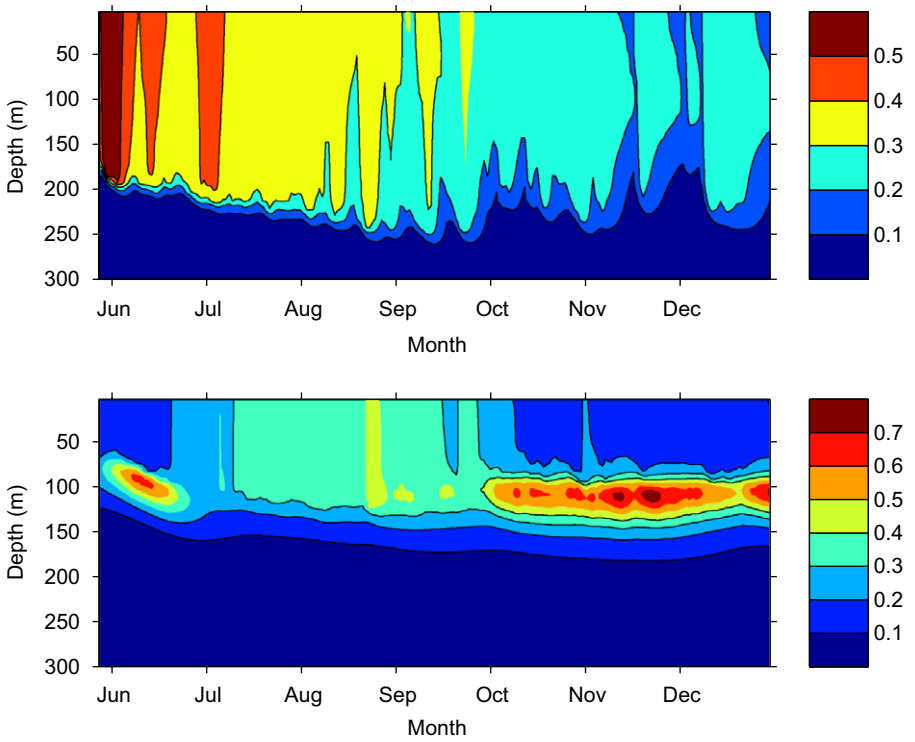

Fig. 14. Model simulated variation in vertical chlorophyll distribution (mg m^{-3}) for the WC (upper panel) and CC (lower panel) eddy between June and December 2003. Note the different colour scales.

CC1 and WC2 are approximately half of the estimates made from sediment traps during October (Table 3).

Fig. 14 shows the temporal variation in vertical chlorophyll distribution simulated by the model between June and December. The WC eddy is characterized by a fairly even distribution of chlorophyll in the upper 200 m between June and September. During early October, predicted chlorophyll biomass decreases and shoals in response to a decrease in vertical mixing (Fig. 12A). This is followed by an increase in vertical mixing during early November (Fig. 12A) that triggers a deepening in its vertical distribution. This pattern of shoaling/decrease followed by deepening/increase in chlorophyll biomass is repeated again during late November and December. In contrast, predicted chlorophyll biomass for the cold eddy is mostly restricted to the upper 110 m and is characterized by a strong chlorophyll maximum at approximately 100 m depth, both initially during June, and then again between October and December. A deepening of the mixed layer (Fig. 11) and strong vertical mixing (Fig. 12A) apparently prevents a deep chlorophyll maximum from forming between July and September during which time an almost even

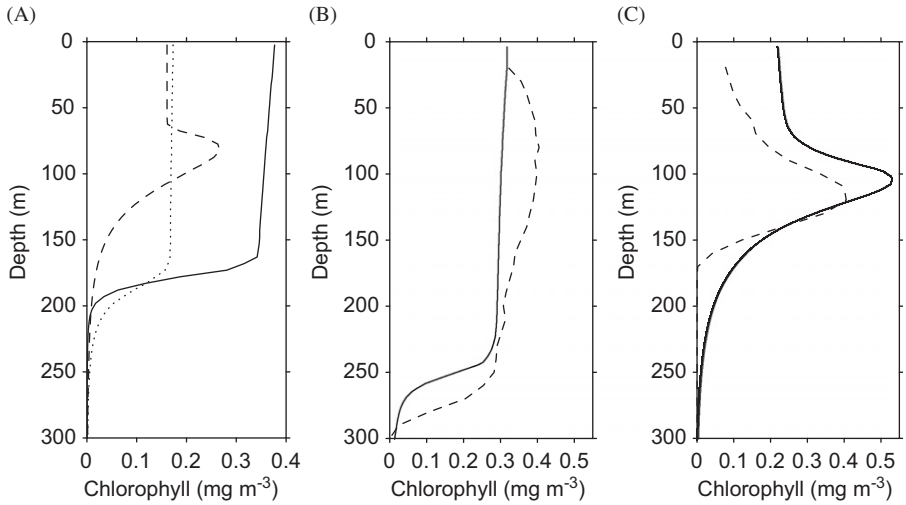

Fig. 15. Vertical profiles of chlorophyll biomass: (A) after 90-day model 'spin-up' for WCl (dotted line); WC2 (solid line); and CCl (dashed line) simulations. Mean model simulated profiles during October (solid line) are compared with observed profiles (dashed line) for (B) WC and (C) CC eddy.

distribution of chlorophyll is simulated by the model throughout the upper 100 m (Fig. 14). Steady shoaling of the mixed layer (Fig. 11), and a sharp decrease in vertical mixing in late September (Fig. 12A) allows a chlorophyll maximum to develop again at the base of the euphotic zone (approximately 100 m). The contrasting vertical chlorophyll structures simulated during October agree well with observations (Fig. 15), although the model tends to underestimate chlorophyll biomass in the WC eddy, and over estimate chlorophyll biomass in the CC eddy.

5. Summary of model results

1. The model successfully captures the vertical temperature structure, and mixed layer depth of the two eddies.
2. Continued flushing with high nutrient surface waters during eddy formation (model 'spin-up') accounts for approximately 75% of the primary production in October in the WC eddy. The influence of this elevated initial total nitrogen content is reduced in November–December.
3. Given the same initial nutrient temperature relationship, production in the CC eddy exceeds that in the WC eddy after approximately 2 months.
4. The best comparison with field data is found in comparing runs WC2 and CC1 for the WC and CC eddies, respectively, highlighting the importance of the nutrient status of surface waters during eddy formation in determining the high biomass and high primary production in the WC eddy.

6. Discussion

We have used a 1-D model to examine the influence of vertical mixing and initial nitrogen conditions on production patterns at the centre of two contrasting eddies, one cyclonic and one anticyclonic. Given appropriate initial conditions, and the same surface forcing, the model successfully distinguishes between the two eddies, reproducing some key features observed during early October 2003. The WC eddy is characterized by a strongly mixed deep surface layer, and a relatively high productivity and vertically even distribution of chlorophyll. In contrast, production in the CC eddy is lower than in the WC eddy and concentrated in a distinct DCM at the top of the nutricline consistent with a shallower mixed layer, and lower rates of vertical mixing.

While our 1-D model has been successful in capturing many observed features of both eddies some limitations of this approach are also apparent in our results. For example, the variability in the observed DIN profile below the mixed layer in the CC eddy (Fig. 6B) suggests that there may by significant vertical and/or horizontal physical processes not included in our model. Furthermore, we

suspect that the poor reproduction of the temporal surface temperature variation in the CC eddy results from vertical mixing in our model being too strong. It has also been speculated that both the SWJ and the STF waters may contribute to the production in the WC by injection of high nitrate water (Waite et al., 2007). The SWJ is a surface trapped feature that contains high phytoplankton biomass that flows southward between the two eddies. From the SST map (Fig. 1), this water mass could wrap the perimeters of both eddies. While the FSLE tells us that there is limited exchange between the cores of the eddies and their perimeters (Fig. 2), ageostrophic flows, such as wind-driven cross-front mixing and subduction may enhance the horizontal mixing in the surface mixed layer.

Further evidence of the influence of horizontal processes is seen in the intrusion of the cold STF waters visible from the SST map (Fig. 1). The STF waters usually possess high nitrate concentration and high phytoplankton biomass (Feng et al., 2007; Waite et al., 2007). There is a possibility that these waters subduct below the mixed layer at the perimeter of the WC eddy (Paterson et al., 2007). Further entrainment of these waters into the core of the WC eddy is unknown. In addition, water subduction below the mixed layer of the WC eddy cannot be discounted. Vertical profile's of water properties in the core of the WC eddy during October reveal a salinity maximum (Fig. 9B) as well as a local silicate maximum just below the WC mixed-layer depth (not shown). Note that this salinity maximum exists in the initial condition of the 1-D model simulation (Fig. 9A), but disappears in the simulation results in October despite weak relaxation of the salinity field to October observations. We conclude that continuous supply of high-salinity water is necessary to maintain this salinity maximum. This continuous supply may also transport additional nutrient to the base of the mixed layer. The importance of advective nutrient supply in supporting production has been identified in similar features elsewhere (e.g., Williams and Follows, 1998; Levy, 2003), and may offer a partial explanation of why biological production and export tends to be underestimated in our model simulations.

Finally, there are also likely to be some biological processes missing from our simple model that contribute to the observed production levels in the two eddies. For example, the ability of some algae species to migrate vertically through the water column to access deep nutrients, or adjust their carbon chlorophyll ratios, may account for some of the mismatch between model and observations particularly for the WC eddy. Similarly, our static light-saturation model does not account for variability in the phytoplankton growth light response, and this may further contribute to an underestimation of production (Macedo and Duarte, 2006).

Despite the limitations of the 1-D approach discussed above, and the underestimation of primary production and export, comparison of production between the two eddies has allowed a useful analysis of the influence that the initial total nitrogen content has in determining subsequent production. Results suggest that the incorporation of productive surface waters during the formation of LC-WC eddies plays an important role in supporting the high observed productivity of the LC-WC eddies as they move off-shore. We propose that entrainment of shelf waters containing relatively high levels of DIN and particulate organic nitrogen during the formation of the LC-WC eddies is the mechanism most likely to explain this result. In contrast, the relatively low production of the CC eddies is best simulated when low surface nutrient conditions, probably more representative of nutrient-poor offshore waters, are supplied during model 'spin-up'. Although, not investigated here, the continued flushing of the WC eddy between its formation in May and its eventual detachment from the LC in August may further impact on its nutrient status and therefore biological production. Given the dramatic effect of elevated initial nutrient, plankton, and detrital levels on subsequent production seen in this study, continued entrainment of high nitrogen shelf waters between formation and detachment of the WC eddy is also likely to have a significant impact on production of the LC-WC eddies.

In an attempt to find an explanation for why production in the CC eddy rapidly exceeds that in the WC eddy when the initial nutrient temperature condition is the same (WC1 and CC1), we have used a Richardson number based diffusivity estimate to calculate the nitrate flux across the base of the mixed layer from observations. The Richardson number is defined as $Ri = N^2/({u_z}^2 + + {v_z}^2)$, where N is the buoyancy frequency derived from the CTD measurements, and u_z and v_z are the vertical shears for zonal and meridional velocities derived from ADCP measurements made during the October eddy cruise. At the base of the mixed layer, the CC

is more stratified than the WC, so that the value of N is higher. At the same time, the vertical shear at the base of the mixed layer is higher in the WC eddy (Feng et al., 2007). Both factors determine that the Richardson number at the base of the WC mixed layer is lower than that in the CC. Following Large et al. (1994), we derive the vertical diffusivity from Ri, that is, $K_z = 10^{-5} + 5 \times 10^{-3}[1-(Ri/Ri_0)^2]^3\,m^2\,s^{-1}$, where $Ri_0 = 0.7$ and $0 \leqslant Ri/Ri_0 \leqslant 1$. The vertical diffusivities below the base of the mixed layer are 2.2×10^{-4} and $1.0 \times 10^{-4}\,m^2\,s^{-1}$ for the WC and CC eddy, respectively. The observed vertical gradients of nitrate are 0.018 and 0.059 mmol $N\,m^{-4}$, respectively, for the WC and CC, so that the resultant nitrate fluxes across the base of the mixed layer are 3.4×10^{-4} and 5.2×10^{-4} mol $N\,m^{-2}\,day^{-1}$, respectively. For comparison, nutrient flux across the base of the mixed layer also can be calculated from the 1-D model. Mean values of K_z immediately below the mixed layer of the WC and CC eddies during early October are calculated by the model to be 2.7×10^{-4} and $3.0 \times 10^{-4}\,m^2\,s^{-1}$, respectively. Multiplying by model estimated vertical DIN gradients of 0.024 and 0.055 mmol $N\,m^{-4}$, returns flux estimates of 7.0×10^{-4} and 1.5×10^{-3} mol $N\,m^{-2}\,day^{-1}$ for the WC and CC eddies, respectively. These relatively large values, compared with those made above result from model estimated diffusivities below the mixed layer being higher than expected from the Richardson number calculations above. The model also estimates diffusivities below the mixed layer to be higher in the CC eddy than in the WC eddy, a result opposite to that found from the Richardson number calculation. We have been unable to find an adequate explanation for this model result. Despite these differences, both methods suggest that vertical fluxes of nitrogen into the mixed layer of the CC eddy are greater than for the WC eddy. From this result it seems unlikely that the vertical flux of nitrate plays a significant role in driving higher production in the WC eddy (see Waite et al., 2007 for a discussion of the role of diatoms in mediating production patterns).

Higher production in the WC eddy during October is partially attributed in our model to a longer detrital mineralization path length, and availability of regenerated nitrogen. This is reflected by the response of simulated production to changes in the detrital decay rate. Sensitivity studies show that production during early October increases with decay rate; linear regression ($r^2 > 0.99$) yielding a gradient of 709.15 and an intercept of 48.40 for the WC eddy, and a gradient of 114.77 and an intercept of 152.98 for the CC eddy (Fig. 16). The fact that production increases more rapidly in the WC eddy as decay rate increases is consistent with a deeper mixed layer, and a longer residence time of sinking detritus in the mixed layer. As the decay rate approaches $0.02\,day^{-1}$, there is little discernable difference in production between the two eddies (Fig. 16). At decay rates above $0.02\,day^{-1}$ production in the WC eddy exceeds that of the CC eddy while below this value, diapycnal mixing presumably becomes the dominant nutrient supply mechanism, and higher production is seen in the CC eddy. This result is consistent with there being higher vertical fluxes of DIN in the CC eddy. The model responds similarly (although oppositely) to changes in detrital sinking speed (not shown). Our subjective choice of $0.06\,day^{-1}$ for the detrital decay constant combined with a constant sinking speed of $10\,m\,day^{-1}$ represents a mineralization length scale of 167 m. In choosing this value we have compromised between reproducing measured production rates, and matching measured export fluxes during October (Table 3). While we have favoured the former largely because of greater uncertainties in the sediment flux data, it is worth noting that a reduction in decay rate to $0.05\,day^{-1}$ results in export fluxes more closely aligned with trap estimates. Without explicitly including bacterial and ammonium dynamics in the model, further quantification of the role of regenerated nitrogen in supporting production in the WC eddy

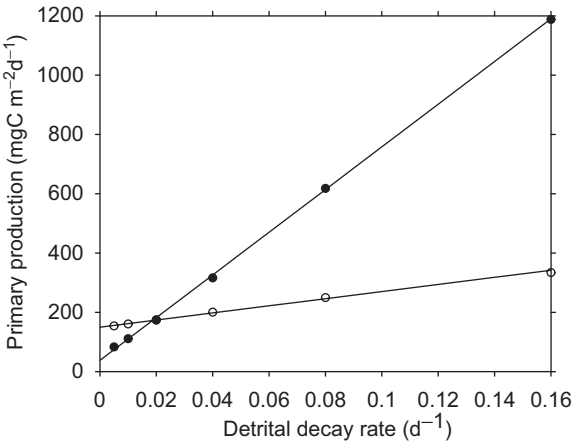

Fig. 16. Response of WC2 and CC eddy primary production during the first half of October to a changing rate of detrital decay.

is not possible. Nevertheless, our model result of a strong dependence of primary production on nitrogen recycling efficiency is consistent with interpretation of phytoplankton and zooplankton data that suggests an important role of microzooplankton grazing in providing recycled nitrogen for continued phytoplankton production in the WC eddy (Paterson et al., 2007). The relative contribution of regenerated nitrogen to total production has also been recognized as an important question within mesoscale eddies in the North Atlantic (e.g., Garcon et al., 2001; Martin and Pondaven, 2003) and encourages further investigation.

In conclusion, results from numerical modelling presented here suggest that the high productivity of anticyclonic eddies that appear along the coast of Western Australia results mainly from a combination of entrainment of productive surface waters containing high levels of dissolved and particulate nitrogen during their formation, and the increased residence time of sinking detritus in the upper mixed layer, while the vertical flux of nitrate from below the mixed layer plays a lesser role.

Acknowledgements

We thank A.P. Martin and one anonymous referee for their detailed and constructive comments that greatly improved the manuscript. We also acknowledge the crew of the Southern Surveyor and the scientists involved in collecting the data used in our analysis. This work was partially funded by the Strategic Research Fund for the Marine Environment.

References

Burchard, H., Baumert, H., 1995. On the performance of a mixed-layer model based on the k–ε turbulence closure. Journal of Geophysical Research 100 (C5), 8523–8540.

Doney, S.C., Glover, D.M., Najjar, R.G., 1996. A new coupled, one-dimensional biological–physical model for the upper ocean: applications to the JGOFS Bermuda Atlantic Time-series Study (BATS) site. Deep-Sea Research II 43, 591–624.

Feng, M., 2006. Eddy induced cross-shelf transport along the downwelling coast off Western Australia. Manuscript, submitted for publication.

Feng, M., Wijffels, S., Godfrey, S., Meyers, G., 2005. Do eddies play a role in the momentum balance of the Leeuwin Current? Journal of Physical Oceanography 35 (6), 964–975.

Feng, M., Fandry, C., Majewski, L., Waite, A., 2007. Characteristics of two counter-rotating eddies in the Leeuwin Current system off the Western Australian coast. Deep-Sea Research II, this issue [doi:10.1016/j.dsr2.2006.11.022].

Fennel, K., Spitz, Y.H., Letelier, R.M., Abbott, M.R., Karl, D.M., 2002. A deterministic model for N_2 fixation at stn. ALOHA in the subtropical North Pacific Ocean. Deep-Sea Research II 49, 149–174.

Garcon, V.C., Oschlies, A., Doney, S.C., McGillicuddy, D., Waniek, J., 2001. The role of mesoscale variability on plankton dynamics in the North Atlantic. Deep-Sea Research II 48, 2199–2226.

Kalnay, E., et al., 1996. The NCEP/NCAR 40-year reanalysis project. Bulletin of the American Meteorological Society 77 (3), 437–471.

Kantha, L.H., 2004. A general ecosystem model for applications to primary production and carbon cycle studies in the global oceans. Ocean Modelling 6 (3–4), 285–334.

Kraus, E.B., 1972. Atmosphere–Ocean Interaction. Clarendon Press, Oxford, UK, p. 275.

Large, W.G., McWilliams, J.C., Doney, S.C., 1994. Oceanic vertical mixing—a review and a model with a nonlocal boundary-layer parameterization. Reviews of Geophysics 32 (4), 363–403.

Levy, M., 2003. Mesoscale variability of phytoplankton and of new production: impact of the large-scale nutrient distribution. Journal of Geophysical Research 108, 3358.

Macedo, M.F., Duarte, P., 2006. Phytoplankton production modeling in three marine ecosystems—static versus dynamic approach. Ecological Modelling 190, 299–316.

Martin, A.P., Pondaven, P., 2003. On estimates for the vertical nitrate flux due to eddy pumping. Journal of Geophysical Research 108, 3359.

McGillicuddy Jr., D.J., McCarthy, J.J., Robinson, A.R., 1995. Coupled physical and biological modeling of the spring bloom in the North Atlantic (I): model formulation and one dimensional bloom processes. Deep-Sea Research I 42, 1313–1357.

McGillicuddy Jr., D.J., Johnson, R., Siegel, D.A., Michaels, A.F., Bates, N.R., Knap, A.H., 1999. Mesoscale variations of biogeochemical properties in the Sargasso Sea. Journal of Geophysical Research 104, 13381–13394.

Moore, T., Matear, R., Marra, J., Clementson, L., 2007. Phytoplankton variability off the Western Australian Coast: Mesoscale eddies and their role in cross-shelf transport. Deep-Sea Research II, this issue [doi:10.1016/j.dsr2.2007.02.006].

Oguz, T., Ducklow, H., Malanotte-Rizzoli, P., Tugrul, S., Nezlin, N.P., Unluata, U., 1996. Simulation of annual plankton productivity cycle in the Black Sea by a one-dimensional physical–biological model. Journal of Geophysical Research 101, 16585–16599.

Paterson, H., Knott, B., Waite, A.M., 2007. Microzooplankton community structure and herbivory on phytoplankton, in an eddy pair in the Indian Ocean off Western Australia. Deep-Sea Research II, this issue [doi:10.1016/j.dsr2.2006.12.011].

Rennie, S.J., Pattiaratchi, C.B., McCauley, R.D., 2007. Eddy formation through the interaction between the Leeuwin Current, Leeuwin Undercurrent and topography. Deep-Sea Research II, this issue [doi:10.1016/j.dsr2.2007.02.005].

Richardson, P.L., 1993. A census of eddies observed in North Atlantic SOFAR float data. Progress in Oceanography 31, 1–50.

Spitz, Y.H., Moisan, J.R., Abbott, M.R., 2001. Configuring an ecosystem model using data from the Bermuda Atlantic Time Series (BATS). Deep-Sea Research II 48, 1733–1768.

Thompson, P., Pesant, S., Waite, A.M., 2007. Contrasting the vertical differences in the phytoplankton biology of a dipole pair of eddies in the south-eastern Indian Ocean. Deep-Sea Research II, this issue [doi:10.1016/j.dsr2.2006.12.009].

Waite, A.M., Thompson, P.A., Pesant, S., Feng, M., Beckley, L.E., Domingues, C., Gaughan, D., Hanson, C., Holl, C., Koslow, J.A., Meuleners, M., Montoya, J., Moore, T., Muhling, B., Paterson, H., Rennie, S., Strezelecki, J., Twomey, L., 2007. The Leeuwin Current and its eddies: An introductory overview. Deep-Sea Research II, this issue [doi:10.1016/j.dsr2.2006.12.008].

Williams, R.G., Follows, M.J., 1998. Eddies make ocean deserts bloom. Nature 394, 228–229.